AIAA JOURNAL
Vol. 35, No. 10, October 1997

Direct Computation of Mach Wave Radiation in an Axisymmetric Supersonic Jet

Brian E. Mitchell,* Sanjiva K. Lele,† and Parviz Moin‡
Stanford University, Stanford, California 94305

The intense Mach waves radiated by the growth and decay of linear instability waves in the shear layer of a perfectly expanded, axisymmetric jet with an initial centerline Mach number of $M_j = 2.0$ are directly computed by solution of the compressible Navier–Stokes equations on a computational domain that includes both the near and far fields. The directly computed far-field sound is compared to predictions obtained using an analysis based on linear stability theory, Lighthill's equation, and the Kirchhoff surface method. All of the predictions are in good agreement with the direct computations. Using Lighthill's equation, we demonstrate that it is essential to properly address the acoustical noncompactness of the sources. It is also shown that linear stability theory can be used to specify the source terms in Lighthill's equation; the resulting predictions are also in good agreement with the computations.

Nomenclature

$\hat{A}$	= constant used in Tam–Burton analysis
c_∞	= speed of sound at ambient conditions
f, f_0	= temporal frequency, fundamental frequency
$\hat{g}(\eta)$	= spatial Fourier transform of instability wave
k	= spatial wave number in x_1
M_j	= Mach number of jet, $M_j = U_0/c_\infty$
R_s	= radius of Kirchhoff surface
R_0	= jet radius
r	= radial coordinate
U_0	= centerline velocity of the jet at $x_1 = 0$
$\hat{u}$	= Fourier transform of axial velocity disturbance
x_1	= axial coordinate
α	= integrated growth rate used in Tam–Burton analysis
β	= nonparallel flow correction factor used in Tam–Burton analysis
δ_2	= momentum thickness
ϵ	= small parameter in Tam–Burton analysis
η	= spatial frequency used in Tam–Burton analysis
Θ	= dilatation, $\Theta = \nabla \cdot \boldsymbol{u}$
θ	= angle measured with respect to x_1 axis
$\lambda(k, \omega)$	= "radial wave number" used in Tam–Burton analysis
ω	= temporal wave number

Subscripts

inner	= inner solution in Tam–Burton analysis
outer	= outer solution in Tam–Burton analysis

Superscripts

$'$	= disturbance quantity
$\bar{}$	= time-averaged quantity
$\hat{}$	= Fourier-transformed (in time) quantity
$\tilde{}$	= linear-stability eigenvector

Received Nov. 12, 1996; revision received June 13, 1997; accepted for publication July 3, 1997.

*Research Assistant, Department of Mechanical Engineering; currently Mechanical Engineer, General Electric Corporate Research and Development Center, P.O. Box 8, Schenectady, NY 12301. Member AIAA.

†Assistant Professor, Department of Mechanical Engineering and Department of Aeronautics and Astronautics. Member AIAA.

‡Franklin and Caroline Johnson Professor of Engineering, Department of Mechanical Engineering, and Senior Staff Scientist, NASA Ames Research Center, Moffett Field, CA 94035. Associate Fellow AIAA.

I. Introduction

THE sound radiated by supersonic jets has received renewed interest in recent years, e.g., Refs. 1–3, because of the development of new supersonic aircraft. The noise from supersonic jets generally is viewed to arise from three sources: 1) mixing noise, 2) screech, and 3) broadband shock noise.[1] The goal of the present study is to continue our work,[4,5] in which we directly computed the far-field sound generated by vortex pairing in axisymmetric jets, to investigate mixing noise in an unheated, axisymmetric jet with an initial centerline Mach number of $M_j = 2$.

Recent theoretical investigations have described mixing noise in terms of the growth and decay of instability waves that give rise to intense Mach-wave radiation.[6–12] The angle of these intense conical waves can be estimated as $\sin(\psi) = 1/M_i$, where M_i is the Mach number relative to the ambient medium at which disturbances are propagating in the shear layer and where the angle ψ is defined in Fig. 1. Tam and Burton,[10,11] hereafter referred to as T&B, present an analysis based on linear stability theory that relates the far-field sound to the growth and decay of instability waves in the jet shear layer.

Although the use of linear stability theory is quite appealing because it seeks to include the underlying physics of the problem, it certainly is not the only approach to predicting supersonic mixing noise. Two other available approaches are Lighthill's equation[13,14] and the Kirchhoff surface method.[15–18] These methods were considered in our earlier investigation of the sound generated by vortex pairing,[4] where they were shown to be in good agreement with the directly computed far-field sound.

We present the results of two computations of a perfectly expanded (to avoid shock-associated noise), unheated, axisymmetric jet with an initial centerline Mach number of $M_j = U_0/c_\infty = 2.0$, Reynolds number $Re = \rho_0 R_0 U_0/\mu = 2.5 \times 10^3$, Prandtl number $Pr = 1$, and initial momentum thickness of $\delta_2/R_0 = 0.05$. The computations differ only in the frequency at which small spatially growing disturbances are introduced. In the first simulation, the inflow boundary of the computation is excited at the fundamental frequency f_0, which is the frequency at which inviscid linear stability theory[19] predicts that disturbances should be most amplified (based on the parallel flow assumption and using the velocity profile at the inflow boundary). The second simulation was excited at the first subharmonic frequency $f_0/2$. The Strouhal number of the fundamental frequency is $Sr_0 = f_0 R_0/U_0 = 0.18$, and the magnitude of the forcing is sufficiently small that the disturbances grow and decay in a linear regime. This is precisely the physical situation considered by T&B. The directly computed results are compared to predictions obtained using the analysis of T&B, Lighthill's equation, and the Kirchhoff surface method. Note from the outset that the axisymmetric instability modes considered herein are not necessarily the

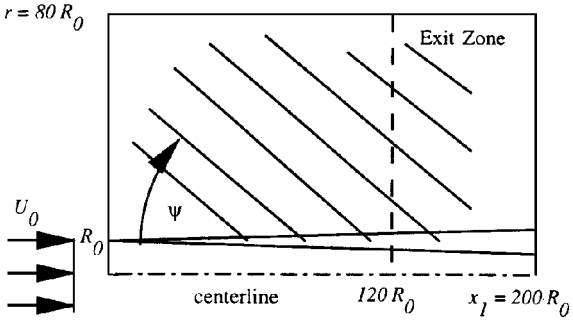

Fig. 1 Schematic of computational domain.

dominant instability modes in high-speed jets (see, e.g., the experiments of Troutt and McLaughlin[20]). However, even when it is not the dominant instability mode, the axisymmetric mode is nevertheless important and affords a computationally inexpensive model problem to study prediction methods for supersonic mixing noise.

In Sec. II, we briefly summarize the numerical procedures. In Sec. III, we present the results of the numerical simulations. The three acoustic theories (T&B, Lighthill's equation, and the Kirchhoff surface method) are reviewed in Secs. IV.A–IV.C, and predictions obtained using these theories are compared to the direct numerical simulation (DNS) data in Sec. IV.D. The results are summarized in Sec. V.

II. Numerical Method

Because the numerical method used in the current study is nearly identical to the method used in Ref. 4, it is summarized only briefly. A schematic of the computational domain is shown in Fig. 1, where it can be seen that the domain includes the region $0 \leq x_1 \leq 200R_0$ and $0 \leq r \leq 80R_0$. The grid is uniform in the x_1 direction with spacing $\Delta x_1 = 0.17R_0$. In the r direction, the grid has spacing $\Delta r = 0.03R_0$ in the near field and spacing $\Delta r = 0.30R_0$ in the far field. The governing equations are the compressible Navier–Stokes equations with the assumption of constant viscosity. Spatial derivatives are discretized with fourth-order-accurate Padé schemes,[21] and time advancement is with the standard fourth-order Runge–Kutta algorithm with time step $\Delta t U_0/R_0 = 1/(128Sr_0)$. Initial conditions are obtained by solving the compressible boundary-layer equations.

The nonreflecting boundary conditions of Giles[22,23] are used. To avoid the generation of spurious acoustic waves as near-field disturbances reach the downstream boundary at $x_1 = 200R_0$, the computations are run only until the first disturbances reach the downstream boundary. By this point in time, the region $0 \leq x_1 \leq 120R_0$ has already become periodic in time. Thus, all data considered in this paper are from the region $0 \leq x_1 \leq 120R_0$. The region $120R_0 \leq x_1 \leq 200R_0$ serves as an exit zone.

Because the data are periodic in time, it is convenient to present the data in terms of Fourier transforms, e.g.,

$$p(x_1, r; t) = \sum \hat{p}(x_1, r; \omega_n) e^{i\omega_n t}$$

III. Results

Figure 2 shows the axial development of the momentum thickness δ_2. The momentum thickness grows quite rapidly at first; in fact, the shear layer doubles in thickness in the first nine jet radii. (Note that the wavelength of the disturbances at the first subharmonic frequency is $9.3R_0$.)

The growth of near-field disturbances is shown in Fig. 3. The disturbances grow initially, peak, and then decay. For the fundamental frequency, the peak occurs at $x_1 = 25R_0$, where the disturbance amplitude is approximately 2.5 times the initial amplitude. For the first subharmonic frequency, the peak occurs at $x_1 = 53R_0$, where the disturbance amplitude is approximately five times the initial amplitude. Note from Fig. 2 that the mean flow is not modified by the growth or decay of disturbances. Fourier transforms verified that the near field is dominated by a single frequency, either the fundamental or the first subharmonic, depending on the simulation. The wiggle in $|\hat{u}|$ at the fundamental frequency seen in Fig. 3a is due

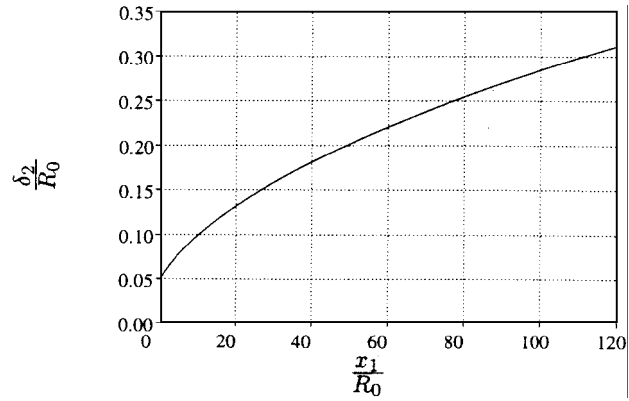

Fig. 2 Axial growth of momentum thickness: ——, DNS and – – –, laminar initial condition (curves are on top of one another).

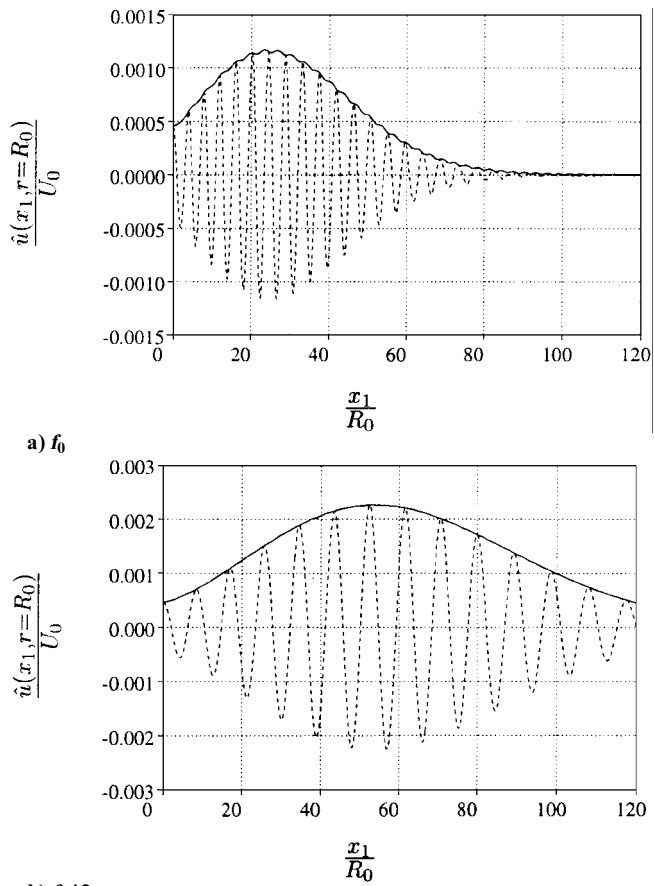

Fig. 3 Growth of axial velocity disturbances $\hat{u}$ at $r = R_0$: – – –, real ($\hat{u}$) and ——, $|\hat{u}|$.

to the presence of a second instability mode. We have verified that this second mode is not due to the numerical method or boundary conditions. Although the physical nature of this second mode has not been investigated, supersonic jets are known to support multiple instability modes.[24]

By performing additional simulations in which the initial amplitude of the disturbances was reduced, we were able to show that disturbances are growing linearly, i.e., the peak level of the disturbances scales with the initial amplitude of the disturbance. These simulations also showed that the magnitude of the far-field sound scales with the initial amplitude of disturbances.

Instantaneous pictures of the far-field sound are shown in Fig. 4, where we defined the far field as the region of the flow where the Navier–Stokes equations reduce to the linearized Euler equations (see Refs. 4 and 5 for more details). Note the intense Mach-wave radiation in Fig. 4. Comparing Figs. 4a and 4b, it is evident that the computational domain is not large enough to show the fully

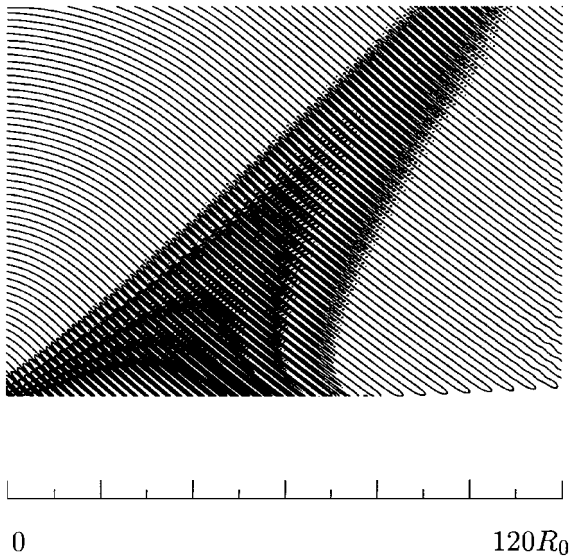

a) Excited at fundamental frequency, the contours of the far-field dilatation $\Theta R_0/c_\infty$ ranging from $\pm 2 \times 10^{-3}$ with increment 4×10^{-4}

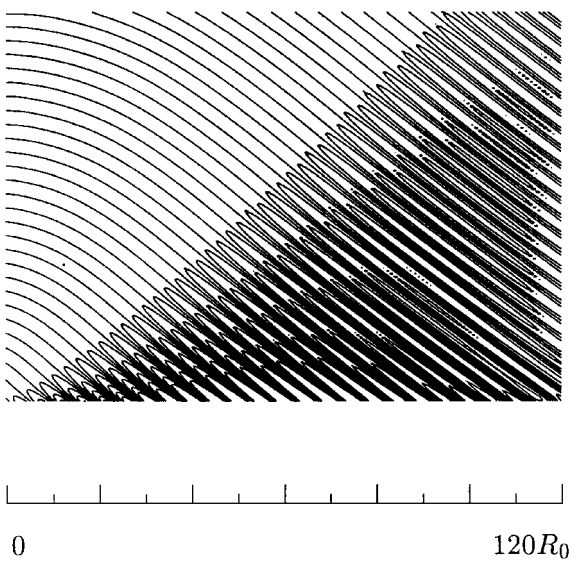

b) Excited at first subharmonic frequency, the contours of the far-field dilatation $\Theta R_0/c_\infty$ ranging from $\pm 1.5 \times 10^{-3}$ with increment 3×10^{-4}

Fig. 4 Instantaneous ($tc_\infty/R_0 = 222$) far-field dilatation for the supersonic jet. (Lower boundary is at $r = 2R_0$, and upper boundary is at $80R_0$; vertical scale is identical to horizontal scale.)

developed far-field pattern at the first subharmonic frequency, i.e., the axial extent of the computational domain is not large enough to contain the quiet region downstream of the most intense Mach-wave radiation. With reference to Fig. 1, the angle of the Mach waves is $\psi \approx 40$ deg. This is in good agreement with the estimate $\sin(\psi) = 1/M_i$, where M_i is the Mach number at which instabilities are propagating. In the present case, linear stability theory shows that $M_i \approx 1.5$. Fourier transforms of the dilatation revealed that the far field is dominated by a single frequency, either the fundamental or the first subharmonic, depending on the simulation.

The directivity of the far-field sound is shown in Fig. 5. In this figure, the dilatation at a distance x from the origin ($x_1 = r = 0$) is plotted vs angle (θ) from the downstream x_1 axis. Of particular interest is the large variation in the magnitude of the far-field sound with angle. Once again, note that the computational domain is not large enough to capture the fully developed far-field sound at the first subharmonic frequency.

Finally, we note that an additional simulation was performed using a smaller computational domain but with the grid spacing reduced by a factor of two in both directions. The results of this additional computation agreed with the results reported earlier, in

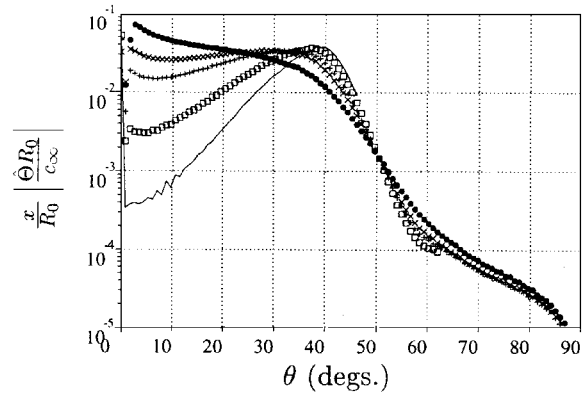

a) Fundamental frequency

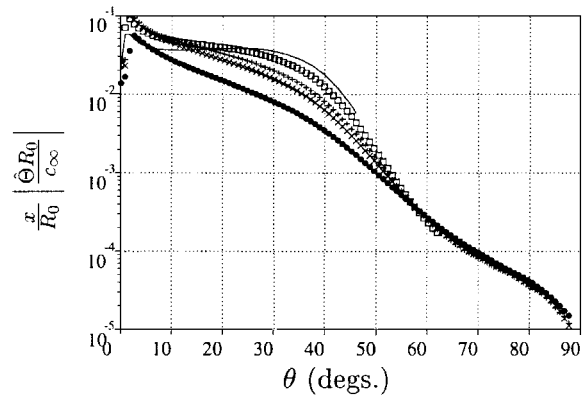

b) First subharmonic frequency

Fig. 5 Magnitude of Fourier transform of the far-field dilatation $\Theta = \nabla \cdot \mu$ at various distances x from the origin measured vs angle θ from the downstream axis: ●, $x = 40R_0$; ×, $x = 60R_0$; +, $x = 70R_0$; □, $x = 90R_0$; and ——, $x = 110R_0$.

particular for the growth of the axial velocity disturbances and the far-field dilatation, to within an accuracy of 5%.

IV. Prediction Methods

In the following three subsections, we summarize the theory of T&B, Lighthill's equation, and the Kirchhoff surface method. Some results pertinent to the individual methods are presented in these subsections, and the far-field predictions from each method are presented together in Sec. IV.D.

A. T&B Analysis

The T&B method (see also summary in Ref. 12) is based on a matched asymptotic expansion between an inner solution determined by use of linear stability theory and an outer solution satisfying the wave equation. The theory predicts the sound generated by a single spatially evolving instability wave of temporal frequency ω. The inner solution is given by

$$\hat{P}_{\text{inner}}(x_1, r; \omega) = i\hat{A}\tilde{p}(r; x_1)\exp[i\alpha(x_1) - \beta(x_1)] \qquad (1)$$

where

$$\alpha(x_1) = \int_0^{x_1} k(y_1)\,dy_1$$

The arbitrary constant $\hat{A}$ is determined with reference to the simulation. The eigenvector $\tilde{p}$ and eigenvalue k are determined via parallel-flow linear stability theory using the mean profiles at x_1. Note that α and k are complex. (The normal modes used in linear stability analysis are of the form $p' = \tilde{p}e^{-i\omega t + ikx_1}$.) The eigenvector is normalized such that, for large r,

$$\frac{\tilde{p}(r; x_1)}{\rho_0 U_0^2} \approx H_0^{(1)}(i\lambda r) \qquad (2)$$

where $\lambda(k, \omega) = [k^2 - (\omega/c_\infty)^2]^{1/2}$ and where $H_0^1(x)$ is the zeroth-order Hankel function of the first kind.

The far-field solution is given by the Fourier integrals

$$\hat{P}_{\text{outer}}(x_1, r; \omega) = i\hat{A}\int_{-\infty}^{\infty} \hat{g}(\eta) H_0^{(1)}[i\lambda(\eta; \omega)r] e^{i\eta x_1}\, d\eta \quad (3)$$

where

$$\hat{g}(\eta) = \frac{1}{2\pi}\int_{-\infty}^{\infty} \exp[i\alpha(x_1) - \beta(x_1)] e^{-i\eta x_1}\, dx_1 \quad (4)$$

In comparing with the simulation, the predicted far-field pressure fluctuations can be converted to dilatation fluctuations via $\hat{\Theta}_{\text{TB}} = [i\omega/(\rho_\infty c_\infty^2)]\hat{P}_{\text{outer}}$. When computing P_{outer} and $\hat{g}$, the infinite limits on the Fourier integrals are truncated, i.e., the Fourier integrals are converted into Fourier transforms defined over the region $0 \le x_1 \le 500R_0$ (the data are zero padded in the region $120R_0 \le x_1 \le 500R_0$). The Fourier transforms then are computed using the fast Fourier transform algorithm.

All that remains is the specification of the constant $\hat{A}$. It is convenient to specify this constant in terms of the level of the axial velocity disturbance at $x_1 = 0$:

$$\hat{A} = \frac{\hat{a}}{\rho_0 U_0 \tilde{u}(x_1 = 0, r = R_0)} \quad (5)$$

The complex constant $\hat{a}$ is determined from the simulation from which it is given by the measured value of $\hat{u}(x_1 = 0, r = R_0)$, i.e., $\hat{a} = \hat{u}(0, R_0)$. This ensures that $\hat{U}_{\text{inner}}$ matches the measured value of $\hat{u}$ at the point $(x_1 = 0, r = R_0)$.

The T&B analysis is accurate to leading order, i.e., the error is order ϵ, where ϵ is a (preferably small) parameter that describes the growth rate of the shear layer. We estimate $\epsilon = (R_0/\delta_2)(d\delta_2/dx_1) = 0.16$ on the basis of flow conditions at $x_1 = 0$.

Typically, linear stability analysis of jets neglects the influence of viscosity. However, we found that the linear stability of the jet considered in this study is influenced strongly by the viscosity. Figure 6 plots the growth rate of disturbances vs the (time) frequency of the disturbances. Shown are linear stability predictions obtained using the (inviscid) Rayleigh equations,[19] the quasi-Orr–Sommerfeld (QOS) equations, and the compressible Orr–Sommerfeld equations. The QOS equations are developed by neglecting the energy equation and using the incompressible form of the viscous terms in the momentum equations. This is the approach used at low Mach number in Ref. 25. (For $\omega = 0$, the equations are given in Ref. 26.) The compressible Orr–Sommerfeld equations are the logical axisymmetric version of the equations used in Ref. 27. It is evident that viscosity is important in this problem and that the QOS equations are an excellent approximation to the compressible Orr–Sommerfeld equations. (The Orr–Sommerfeld equations could not be solved for larger frequencies because of numerical difficulties that arise when the energy equation is nearly decoupled from the momentum equations.)

The prediction for the growth of near-field disturbances is shown in Fig. 7. At both frequencies, the predictions peak earlier than the

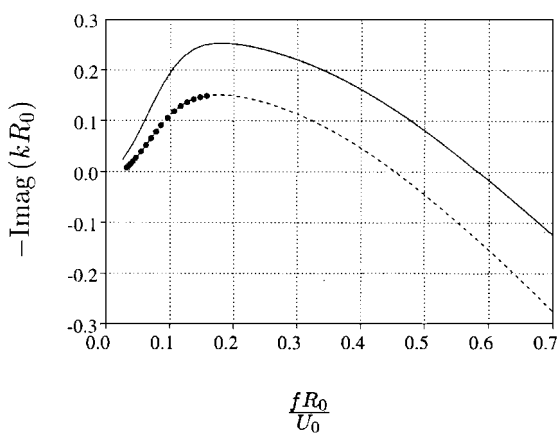

Fig. 6 Predicted growth rate of disturbances obtained from parallel-flow linear stability theory using the mean velocity profile at $x_1 = 0$: ——, inviscid theory (Rayleigh equation); – – –, viscous theory using the QOS equations; and ●, viscous theory using full compressible Orr–Sommerfeld equations.

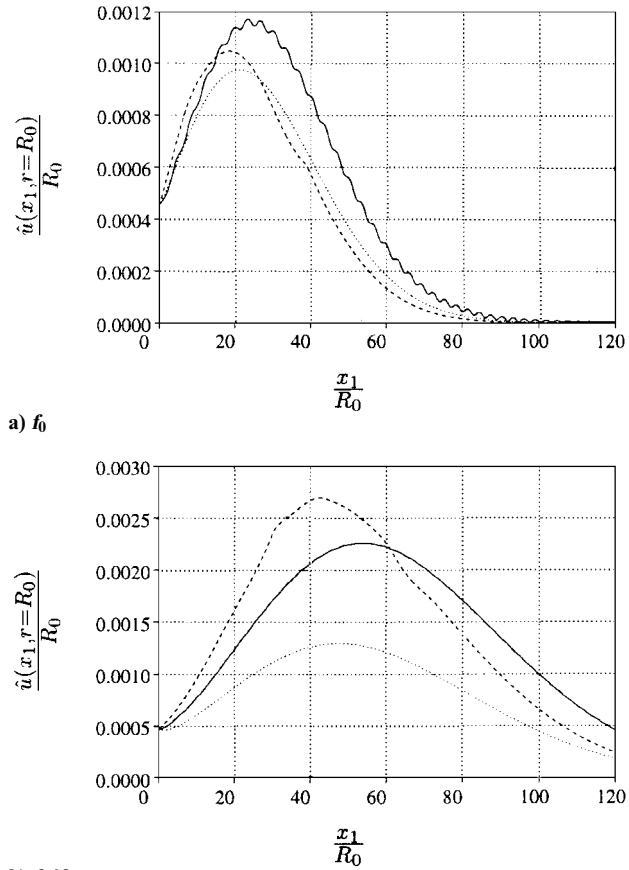

Fig. 7 Growth of axial velocity disturbances $\hat{u}$ at $r = R_0$: ——, DNS; – – –, T&B analysis; and ..., T&B analysis with $\beta(x_1) = 0$.

DNS data. At the fundamental frequency, the peak amplitude is underpredicted by approximately 10% and at the first subharmonic the peak amplitude is overpredicted by approximately 15%. These errors are consistent with our estimate of $\epsilon = 0.16$. Also shown in Fig. 7 is the prediction obtained by neglecting the nonparallel-flow correction factor $\beta(x_1)$. Note that β is more important at the first subharmonic frequency. This is expected because the wavelength of the instabilities is longer at lower frequencies and thus the mean flow changes more per instability wavelength. In fact, at the first subharmonic frequency, the momentum thickness doubles during the first wavelength of the instability.

B. Lighthill's Equation

Lighthill's equation[13] is an exact rearrangement of the continuity and momentum equations:

$$\frac{\partial^2 \rho'}{\partial t^2} - \nabla_{(y)}^2 \rho' = \frac{\partial^2}{\partial y_i \partial y_j} T_{ij}(\mathbf{y}; t) \quad (6)$$

where the Lighthill stress tensor T_{ij} is given by

$$T_{ij} = \rho u_i u_j + (p' - c_\infty^2 \rho')\delta_{ij} - \tau_{ij} \quad (7)$$

where τ_{ij} are the viscous stresses and the primes represent fluctuations about ambient values, e.g., $\rho = \rho_\infty + \rho'$. As written, Eq. (6) is an exact equation; approximation is introduced when the right-hand side is specified independently and the left-hand side then is solved for the far-field sound. We neglect the contribution of the viscous terms to T_{ij}. A component of the Lighthill stress tensor is shown in Fig. 8; the source term has a Gaussian-like shape. The ρuu component is the largest component of the stress tensor.

Our solution procedure is described in Refs. 4 and 5. In brief, the solution of the Fourier transform of Eq. (6) is expressed in terms of its Green's function, and the resulting convolution integral is solved numerically without any assumption about acoustical compactness. Note that the model introduced in Refs. 4 and 5 to handle the slow

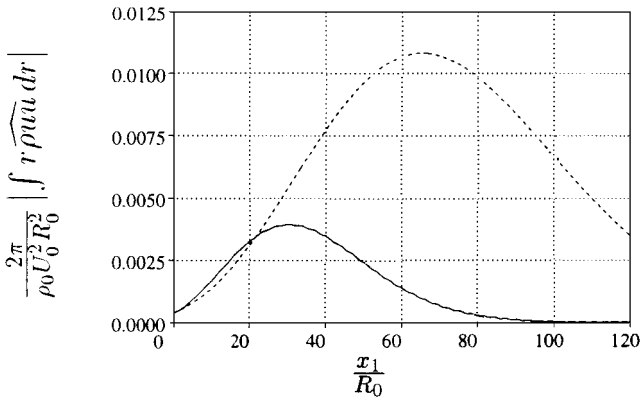

Fig. 8 Magnitude of Fourier transform of a component of the Lighthill source term ρuu integrated in the radial direction: ——, f_0 and – – –, $f_0/2$.

decay (in x_1) of the Lighthill stress tensor is not needed in the present study. The radial integrals are truncated at $r = 5R_0$.

C. Kirchhoff Surface Method

The Kirchhoff surface method for predicting sound is based on an analytical formula that relates the far-field sound to integrals over a closed surface that surrounds all acoustic sources. As the computation is run, the dilatation is saved at the location of the surface; numerical quadrature then is performed to find the far-field sound. The formulation used here is identical to that described in Refs. 4 and 5. Lyrintzis[16] reviews other recent aeroacoustic applications.

For the jet computations, the surface used is a cylinder of radius R_s and axial extent $0 \leq x_1 \leq 120R_0$. Because the flow in the jet's shear layer does not obey the acoustic equations (it is, of course, governed by the Navier–Stokes equations), the endcaps of the cylinder cannot be included in the Kirchhoff surface. An alternative viewpoint is that the ideal Kirchhoff surface should be infinite in the axial direction but must be limited to a finite length that matches the available computational information. Regardless of the view taken, part of the Kirchhoff surface is left open, and it is well known that errors should be expected (see, e.g., Refs. 17 and 18). Freund et al.[17] discuss the errors associated with using an open Kirchhoff surface and show mathematically that, if the ray between the far-field observer and the acoustic source intersects part of the included surface, then errors from the missing surface should not dominate the predicted sound. As discussed in Sec. IV.D, very quiet regions of the flow, such as seen in the present investigation for $\theta > 50$ deg, are more sensitive to errors from the use of an open surface.

An important issue is the appropriate radial location of the Kirchhoff surface. In our earlier work,[4] the location of the Kirchhoff surface was chosen by comparing the Euler and Navier–Stokes equations to determine where the Navier–Stokes equations reduce to the wave equation. Such comparisons in the present study suggest that the Kirchhoff surface can be located as close as $R_s = 4R_0$. The results presented in this paper were obtained for $R_s = 7R_0$.

D. Comparison of Predictions to DNS

Predictions obtained using the analysis of T&B, Lighthill's equation, and the Kirchhoff surface method are compared to the DNS data in Fig. 9. All of the methods are in good agreement with the DNS data. The slightly larger differences between the results obtained using the analysis of T&B and the DNS data are due to the fact that the parameter ϵ is not especially small (recall that ϵ was estimated as 0.16).

Note that the DNS data took a few hours of supercomputer time to compute and the Lighthill and Kirchhoff surface methods (using DNS source data) took a few minutes of additional supercomputer time to compute. The results using the analysis of T&B took a few minutes of supercomputer time to predict and (to within a constant) did not require data from the DNS to compute. Thus the T&B analysis was by far the least expensive result to compute.

Also shown in Fig. 9 is a prediction from Lighthill's equation that was obtained by specifying the Lighthill stress tensor using the

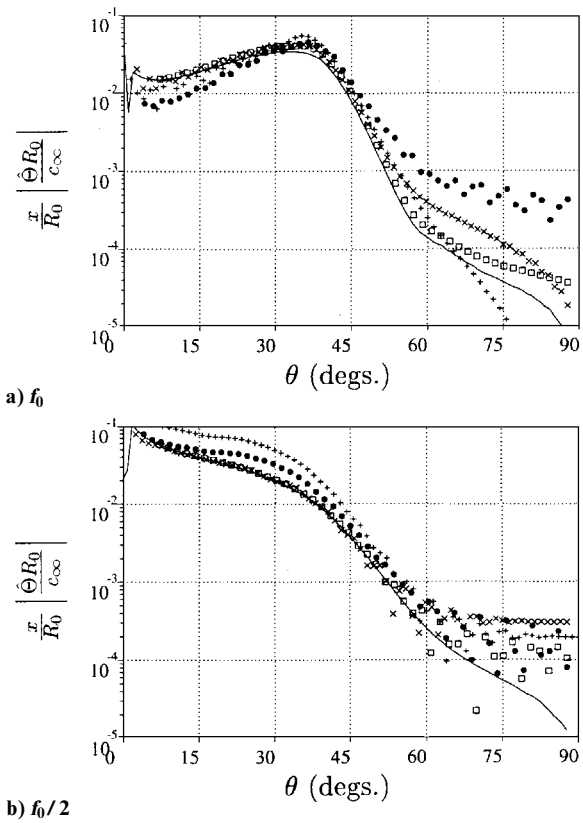

Fig. 9 Comparisons of predictions for the far-field dilatation to the directly computed results at a distance of $x = 70R_0$ away from the origin: ——, DNS; ●, T&B; ×, Lighthill's equation; +, Lighthill's equation where the stress tensor has been specified using linear stability theory; and □, Kirchhoff surface method.

results of linear stability theory, i.e., the inner solution of the T&B analysis summarized in Sec. IV.A. For example, the ρuu component is given by

$$\widehat{\rho uu} = \hat{A}(2\bar{\rho}\tilde{u} + \tilde{\rho}\bar{u}^2)e^{i\alpha - \beta}$$

where $\hat{A}$, α, and β are defined in Sec. IV.A and where only terms that are linear in $\hat{A}$ have been retained. We checked to make sure that the fact that the eigenvectors are not bounded for large r once the instabilities start to decay (see Refs. 10 and 11 for details) does not affect the solution method. Specifically, we found that the predictions were independent of the choice of upper limit in the radial direction source convolution integral if the upper limit $\sigma_{\max}$ was in the range $3R_0 \leq \sigma_{\max} \leq 7R_0$. The predictions obtained with this approach are similar to the T&B results. This approach is an alternative to the T&B analysis for using linear stability theory to predict the far-field sound.

Note that the usual arguments that linear source terms represent the interaction of acoustic waves with the mean flow and not sound generation (see, e.g., the review of low-Mach-number, boundary-layer noise in Ref. 28) do not apply in the present situation because the spatial scales of the acoustic waves and the instability waves are not separated as they would be in a low-Mach-number flow. This is because the instability waves are themselves traveling at supersonic speeds.

The importance of not assuming acoustical compactness in the solution of Lighthill's equation is illustrated in Fig. 10. It is clearly seen that the prediction obtained using the acoustical compactness assumption underpredicts the peak sound levels by two orders of magnitude. Also shown is a prediction obtained from Lighthill's equation that only included the ρuu component of the Lighthill stress tensor. This prediction is in good agreement with the DNS and the prediction obtained using the full stress tensor. This demonstrates that the ρuu component is the most important component in this flow.

All predictions overpredict the far-field sound at large θ, where the sound is less intense. The source of this error is the domain

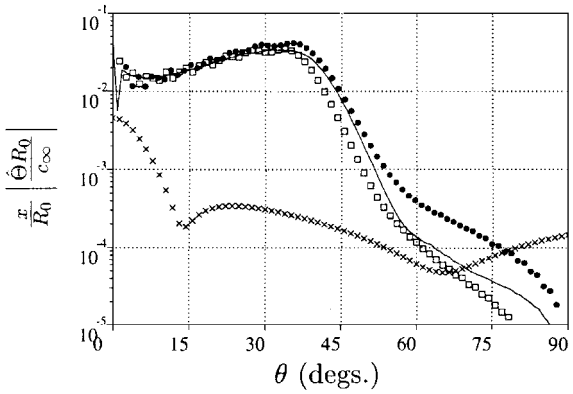

Fig. 10 Comparison of directly computed sound to predictions obtained using various solutions to Lighthill's equations: ——, directly computed sound at a distance of $x = 70R_0$ from the origin at the fundamental frequency; ●, Lighthill's equation; ×, Lighthill's equation solved with the assumption of acoustical compactness; and □, Lighthill's equation solved with only the ρuu component of the Lighthill stress tensor.

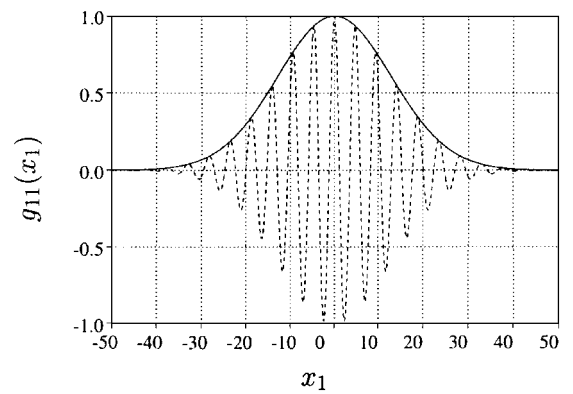

Fig. 11 Gaussian source function g_{11}: ——, magnitude and – – –, real part.

truncation in the x_1 direction. For both the T&B analysis and the solution of Lighthill's equation, the domain truncation takes place when acoustic sources located at $x_1 > 120R_0$ are ignored. For the Kirchhoff surface method, the domain truncation is manifested in the use of an open Kirchhoff surface.

To illustrate the effect of the domain truncation, consider the Helmholtz or reduced wave equation with a source term that is distributed over only one dimension:

$$\nabla^2_{(y)}\hat{\psi} + \left(\frac{\omega}{c_\infty}\right)^2 \hat{\psi} = -\frac{1}{c_\infty^2}\frac{\partial^2}{\partial y_1 \partial y_1}[g_{11}(y_1)\delta(y_2)\delta(y_3)] \qquad (8)$$

The source has a Gaussian shape,

$$g_{11}(y_1) = e^{-\zeta y_1^2}\exp[i(\omega/c_\infty M_k)y_1] \qquad (9)$$

where the various parameters are chosen to be similar to the Lighthill source terms observed in the simulation at the fundamental frequency: $\zeta = 0.003$, $\omega = 2$, and $M_k = 1.5$. The source function is plotted in Fig. 11. The solution of Eq. (8) is

$$\hat{\psi}(x_1, r) = -\frac{\omega^2}{4\pi c_\infty^2}\int_{-L}^{L} g_{11}(y_1)(x_1 - y_1)^2\frac{\exp[i(\omega R/c_\infty)]}{R^3}\,dy_1 \qquad (10)$$

where $R^2 = (x_1 - y_1)^2 + r^2$. Equation (10) is exact in the limit of L approaching ∞. Solutions for different values of L illustrate the influence of source truncation on the far-field sound (Fig. 12). All of the plotted solutions give good results in the region of the far field where the sound is most intense (30 deg $\leq \theta \leq$ 75 deg) but overpredict the part of the far field where the sound is very quiet. The range of good agreement increases with L, but even for the largest L considered, $L = 120$, the solution is accurate only in the range 5 deg $< \theta <$ 100 deg. Note that the source term at $L =$ 120 is extremely small, $g_{11}(120) = 2 \times 10^{-19}$. Physically, the quiet regions of the far field are quiet because of significant cancellation of acoustic waves that were generated over the entire infinite extent of the source. When the source is truncated, the required cancellations do not take place and the sound is overpredicted. This example illustrates the challenge of predicting quiet regions of the far field.

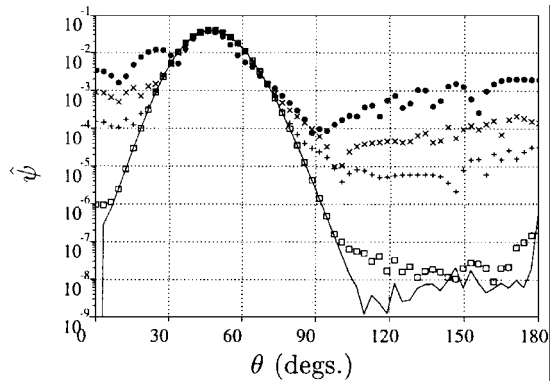

Fig. 12 Far-field sound $\hat{\psi}$ at $x = 70$ generated by the Gaussian source g_{11} (plotted in Fig. 11), computed using Eq. (10) with different upper/lower limits of integration: ● $L = 10$; ×, $L = 30$; +, $L = 40$; □, $L = 60$; and ——, $L = 120$.

V. Summary

The sound radiated by the growth and decay of small-scale disturbances in the shear layer of an unheated, axisymmetric supersonic jet was directly computed by solving the Navier–Stokes equations on a computational domain that includes both the near and far fields. The far-field sound consists of intense Mach waves. The directly computed data were compared to predictions obtained using the analysis of T&B, Lighthill's equation, and the Kirchhoff surface method. All of the predictions are in good agreement with the DNS data. The directly computed far-field sound also was compared to a predictions of Lighthill's equation in which the Lighthill stress tensor was specified using linear stability theory; this prediction was also in good agreement with the DNS data.

Acknowledgments

This work was sponsored by the Office of Naval Research, Grant N00014-92-J-1626, and computer time was provided by the NASA Ames Research Center through the Center for Turbulence Research and by the Numerical Aerodynamic Simulation Program. The first author acknowledges financial support from the Franklin P. and Caroline M. Johnson Fellowship.

References

[1]Tam, C. K. W., "Supersonic Jet Noise," *Annual Review of Fluid Mechanics*, Vol. 27, 1995, pp. 17–43.

[2]Mankbadi, R. R., Hayer, M. E., and Povinelli, L. A., "Structure of Supersonic Jet Flow and Its Radiated Sound," *AIAA Journal*, Vol. 32, No. 5, 1994, pp. 897–906.

[3]Mankbadi, R. R., Hixon, R., Shih, S.-H., and Povinelli, L. A., "On the use of Linearized Euler Equations in the Prediction of Jet Noise," AIAA Paper 95-0505, 1995.

[4]Mitchell, B. E., Lele, S. K., and Moin, P., "Direct Computation of the Sound Generated by Vortex Pairing in an Axisymmetric Jet," AIAA Paper 95-0504, 1995.

[5]Mitchell, B. E., Lele, S. K., and Moin, P., "Direct Computation of the Sound Generated by Subsonic and Supersonic Axisymmetric Jets," Dept. of Mechanical Engineering, Rept. TF-66, Stanford Univ., Stanford, CA, 1995.

[6]Tam, C. K. W., "Directional Acoustic Radiation from a Supersonic Jet Generated by Shear Layer Instability," *Journal of Fluid Mechanics*, Vol. 46, Pt. 4, 1971, pp. 757–768.

[7]Lilley, G. M., "The Generation and Radiation of Supersonic Jet Noise Volume IV.," Lockheed Georgia Co., AFAPL-TR-72-IV, Marietta, GA, 1972, pp. 2–68.

[8]Morris, P. J., "Flow Characteristics of the Large Scale Wave-Like Structure of a Supersonic Round Jet," *Journal of Sound and Vibration*, Vol. 53, No. 2, 1977, pp. 223–244.

[9]Tam, C. K. W., and Morris, P. J., "The Radiation of Sound by the Instability Waves of a Compressible Plane Turbulent Shear Layer," *Journal of Fluid Mechanics*, Vol. 98, Pt. 2, 1980, pp. 349–381.

[10]Tam, C. K. W., and Burton, D. E., "Sound Generated by Instability Waves of Supersonic Flow, Pt. 1, Two Dimensional Mixing Layers," *Journal of Fluid Mechanics*, Vol. 138, 1984, pp. 249–271.

[11]Tam, C. K. W., and Burton, D. E., "Sound Generated by Instability Waves of Supersonic Flow, Part 2, Axisymmetric Jets," *Journal of Fluid Mechanics*, Vol. 138, 1984, pp. 273–295.

[12]Tam, C. K. W., and Chen, P., "Turbulent Mixing Noise from Supersonic Jets," *AIAA Journal*, Vol. 32, No. 9, 1994, pp. 1774–1780.

[13]Lighthill, M. J., "On Sound Generated Aerodynamically, I. General Theory," *Proceedings of the Royal Society of London, Series A*, A211, 1952, pp. 564–587.

[14]Ffowcs Williams, J. E., and Maidanik, G., "The Mach Wave Field Radiated by Supersonic Turbulent Shear Flows," *Journal of Fluid Mechanics*, Vol. 21, Pt. 4, 1965, pp. 641–657.

[15]Kirchhoff, G. R., "Towards a Theory of Light Rays," *Annals of Physical Chemistry*, Vol. 18, 1883, pp. 663–695.

[16]Lyrintzis, A., "A Review of the Uses of Kirchhoff's Method in Computational Aeroacoustics," *Journal of Fluids Engineering*, Vol. 116, Dec. 1994, pp. 665–676.

[17]Freund, J., Lele, S. K., and Moin, P., "Calculation of the Radiated Sound Field Using an Open Kirchhoff Surface," *AIAA Journal*, Vol. 34, No. 5, 1996, pp. 909–916.

[18]Pilon, A. R., and Lyrintzis, A. S., "Integral Methods for Computational Aeroacoustics," AIAA Paper 97-0020, 1997.

[19]Michalke, A., "Survey on Jet Instability Theory," *Progress in Aerospace Science*, Vol. 21, 1984, pp. 159–199.

[20]Troutt, T. R., and McLaughlin, D. K., "Experiments on the Flow and Acoustic Properties of a Moderate-Reynolds-Number Supersonic Jet," *Journal of Fluid Mechanics*, Vol. 116, 1982, pp. 123–156.

[21]Lele, S. K., "Compact Finite Difference Schemes With Spectral-Like Resolution," *Journal of Computational Physics*, Vol. 103, 1992, pp. 16–42.

[22]Giles, M. B., "Non-Reflecting Boundary Conditions for Euler Equations Calculations," *AIAA Journal*, Vol. 28, No. 12, 1990, pp. 2050–2058.

[23]Colonius, T., Lele, S. K., and Moin, P., "Boundary Conditions for Direct Computation of Aerodynamic Sound Generation," *AIAA Journal*, Vol. 31, No. 9, 1993, pp. 1574–1582.

[24]Tam, C. K. W., and Hu, F. Q., "On the Three Families of Instability Waves of High-Speed Jets," *Journal of Fluid Mechanics*, Vol. 201, 1989, pp. 447–483.

[25]Morris, P. J., "Viscous Stability of Compressible Axisymmetric Jets," *AIAA Journal*, Vol. 21, No. 3, 1983, pp. 481–482.

[26]Tam, C. K. W., Jackson, J. A., and Seiner, J. M., "A Multiple-Scales Model of the Shock-Cell Structure of Imperfectly Expanded Supersonic Jets," *Journal of Fluid Mechanics*, Vol. 153, 1985, pp. 123–149.

[27]Mack, L. M., "Computation of the Stability of the Laminar Boundary Layer," *Methods in Computational Physics*, Vol. 4, 1965, pp. 247–299.

[28]Crighton, D. G., Dowling, A. P., Ffowcs Williams, J. E., Heckl, M., and Leppington, F. G., *Modern Methods in Analytical Acoustics*, Springer–Verlag, London, 1992, Chap. 16.

S. Glegg
Associate Editor